THE JOURNAL OF BIOLOGICAL CHEMISTRY VOL. 284, NO. 48, pp. 33265–33274, November 27, 2009

A Double Tyrosine Motif in the Cardiac Sodium Channel Domain III-IV Linker Couples Calcium-dependent Calmodulin Binding to Inactivation Gating[S]

Received for publication, August 5, 2009, and in revised form, September 28, 2009 Published, JBC Papers in Press, October 5, 2009, DOI 10.1074/jbc.M109.052910

Maen F. Sarhan[‡], **Filip Van Petegem**[§1], **and Christopher A. Ahern**[‡1,2]

From the [‡]*Departments of Anesthesiology, Pharmacology and Therapeutics, and Cellular and Physiological Sciences and the* [§]*Department of Biochemistry and Molecular Biology, University of British Columbia, Vancouver, British Columbia V6T 1Z3, Canada*

Voltage-gated sodium channels maintain the electrical cadence and stability of neurons and muscle cells by selectively controlling the transmembrane passage of their namesake ion. The degree to which these channels contribute to cellular excitability can be managed therapeutically or fine-tuned by endogenous ligands. Intracellular calcium, for instance, modulates sodium channel inactivation, the process by which sodium conductance is negatively regulated. We explored the molecular basis for this effect by investigating the interaction between the ubiquitous calcium binding protein calmodulin (CaM) and the putative sodium channel inactivation gate composed of the cytosolic linker between homologous channel domains III and IV (DIII-IV). Experiments using isothermal titration calorimetry show that CaM binds to a novel double tyrosine motif in the center of the DIII-IV linker in a calcium-dependent manner, N-terminal to a region previously reported to be a CaM binding site. An alanine scan of aromatic residues in recombinant DIII-DIV linker peptides shows that whereas multiple side chains contribute to CaM binding, two tyrosines (Tyr^{1494} and Tyr^{1495}) play a crucial role in binding the CaM C-lobe. The functional relevance of these observations was then ascertained through electrophysiological measurement of sodium channel inactivation gating in the presence and absence of calcium. Experiments on patch-clamped transfected tsA201 cells show that only the Y1494A mutation of the five sites tested renders sodium channel steady-state inactivation insensitive to cytosolic calcium. The results demonstrate that calcium-dependent calmodulin binding to the sodium channel inactivation gate double tyrosine motif is required for calcium regulation of the cardiac sodium channel.

Voltage-gated sodium channels control rhythmic firing in excitable cells by driving the rapid upstroke of the action potential. These channels are composed of four homologous domains (DI–DIV), each housing six α-helical transmembrane segments that form the voltage sensor (S1–S4) and the pore-forming (S5-S6) modules. Within a few milliseconds of opening, channels enter a non-conducting, inactivated state from which they must recover before subsequent opening. Sodium channels may also enter this inactivated state directly from the resting state in a voltage-dependent manner (1). It has been suggested that inactivation proceeds through a "hinged lid" mechanism analogous to allosteric enzymes (2) whereby the ~50-amino acid cytoplasmic linker between domains III and IV (DIII-IV)[3] acts as the "lid" to rapidly occlude the permeation pathway. This mechanism is consistent with mutational analysis, where replacement of the DIII-IV linker hydrophobic triplet I^{1485}FM^{1487} with QQQ (3) can substantially reduce the rate and steady-state levels of inactivation. In addition to the DIII-IV linker and its putative binding sites in the S4-S5 linker of domains III (4) and IV (5), the inactivation "complex" includes the C terminus of the channel (6, 7) and the auxiliary β subunit (8). Inactivation can also be regulated by serine/threonine (9) and tyrosine phosphorylation (10) of DIII-IV residues.

Calcium ions in the heart act as an electrochemical link between membrane depolarization and myocyte contraction where their levels can oscillate between submicromolar and micromolar with each excitation-contraction cycle. Sodium channels take advantage of this dynamic environment by allowing Ca^{2+} and calmodulin (CaM) to fine-tune channel availability by making more channels available for each action potential (6, 11, 12). Although the precise mechanistic details of this modulation remain speculative, the C-terminal region contains EF-hand like domains and an IQ motif that dynamically bind Ca^{2+} and Ca^{2+}/CaM, respectively, and mutations in these regions affect both calcium sensitivity and inactivation gating (6, 11, 13–16). Additionally, recent evidence suggests that CaM can bind directly to the DIII-DIV linker, a possibility that has been suggested previously in the context of an "inactivation complex" (14, 17), therefore providing yet another pathway for Ca^{2+}/CaM regulation of channel gating (18). Interestingly, introduced mutations into the putative Ca^{2+}/CaM binding regions in the DIII-IV linker or the IQ motif do not explicitly interfere with calcium modulation of channel inactivation (16, 18), suggesting that Ca^{2+}/CaM binding to the channel *per se* may not play a pivotal role in sensitizing the inactivation pro-

[S] The on-line version of this article (available at http://www.jbc.org) contains supplemental Figs. S1 and S2.

[1] Supported by Canadian Institutes of Health Research Grant 56858, the Heart and Stroke Foundation of Canada, and the Michael Smith Foundation for Health Research.

[2] The 2008–2009 Heart and Stroke Foundation McDonald Scholar. Supported by Canadian Institutes of Health Research Grant 84350, the Heart and Stroke Foundation of Canada, and the Michael Smith Foundation for Health Research. To whom correspondence should be addressed: 2350 Health Sciences Mall, Vancouver, British Columbia V6T 1Z3, Canada. Fax: 604-822-6048; E-mail: cahern@interchange.ubc.ca.

[3] The abbreviations used are: DIII-IV, domain III-IV; CaM, calmodulin; ITC, isothermal titration calorimetry.

cess to calcium. Alternatively, it is possible that CaM binding plays a central role in calcium regulation of inactivation through yet undetermined binding scenarios.

Inherited and acquired dysfunctions of sodium channels can affect the inactivation process and channel modulation by intracellular calcium, respectively (19). The DIII-IV linker and the C terminus of the channel are "hot spot" regions for gain of function mutations that contribute to electrical instability through the generation of a "late" or persistent sodium current that arises when channels fail to completely inactivate (7, 20). Furthermore, Ca^{2+}/CaM has been demonstrated to be a contributing factor in cardiomyopathic calcium dysregulation associated with the emergence of late sodium current that underlies life-threatening cardiac arrhythmia (21, 22). Therefore, the mechanism of sodium channel inactivation and its modulation by calcium is of interest for the management of hyperexcitability disorders and for the general understanding of the basic events that underlie ion channel gating.

Here we employ isothermal titration calorimetry (ITC) to confirm that the sodium channel DIII-IV linker binds CaM with high affinity and show that CaM binding to calcium is required for the interaction, thus adding a novel molecular determinant to calcium regulation of cardiac sodium channels. An alanine scan of the DIII-IV linker shows that aromatic residues support CaM binding, with Tyr^{1494} and Tyr^{1495} being central to the interaction with the calmodulin C-lobe. The biophysical implications of CaM binding to the DIII-IV linker were investigated by patch-clamping tsA201 cells transfected with wild type and DIII-IV mutant channels in high and low calcium. The mutations are well tolerated and generate channels with little or no alteration in their voltage dependence of gating. The results show that the single Y1494A channel mutant is insensitive to cytosolic calcium, whereas mutation of other DIII-IV aromatics produced channels that display calcium-dependent inactivation gating effects. These observations add another mechanistic layer to calcium regulation of the cardiac sodium channel and suggest that Ca^{2+}/CaM binding to the DIII-IV linker is an essential determinant of the regulatory process.

EXPERIMENTAL PROCEDURES

Protein Purification and Isothermal Titration Calorimetry—All recombinant proteins were derived from cDNA from humans. The DIII-IV (Asp^{1471}–Phe^{1522}) was cloned into a modified Pet28 (Novagen) vector. For purification, all constructs included an N-terminal tag of His_6, maltose-binding protein, and a tobacco etch virus cleavage site denoted as an "HMT" tag. Human CaM wild type, N-lobe (residues 1–78), C-lobe (residues 79–148), and CaM1234 (a CaM quadruple Ca^{2+} binding knock-out mutant) were generated previously (23). Plasmids were transformed into BL21 (DE3) cells and grown in 2× YT media at 37 °C and induced with 1 mM isopropyl 1-thio-β-D-galactopyranoside. After centrifugation, pellets were lysed in buffer A (250 mM KCl, 10 mM Hepes, pH 7.4) plus 14 mM β-mercaptoethanol and 1 mM phenylmethylsulfonyl fluoride and were sonicated and then centrifuged. Filtered cell lysate was loaded onto a Talon (Clontech) column, washed with buffer A, and eluted with buffer A plus 500 mM imidazole. Fractions were then run on an amylose column in buffer A and were eluted with buffer A plus 10 mM maltose. His-tagged tobacco etch virus protease was used to cleave the tag for ~12 h. To remove the HMT tag and tobacco etch virus protease, protein solution was run again on the Talon and amylose, in which case the flow-through was collected. To completely remove trace amounts of the HMT tag, a final ion exchange column (Resource Q) was used, using buffer C (10 mM KCl, 20 mM Tris, pH 8.8) and D (1 M KCl, 20 mM Tris, pH 8.8), going from 0 to 40% buffer D over 12 column volumes. Protein integrity and identity were confirmed by both SDS-PAGE and mass spectrometry (electrospray ionization with a quadrupole mass analyzer).

ITC experiments were performed with an ITC-200 (MicroCal) with concentrated, purified protein after dialysis for at least 17 h in 150 mM KCl, 10 mM Hepes (pH 7.4), 14 mM β-mercaptoethanol, and either 1 mM $CaCl_2$, 10 mM $CaCl_2$, or 10 mM EDTA at 25 °C. Protein concentrations were determined by the Edelhoch method (24), where in the case of the N terminus of the CaM N-lobe, which lacks an endogenous aromatic, an engineered tryptophan was used. CaM constructs were used at a 10-fold molar excess when titrated against DIII-IV linker peptides. ITC experiments were repeated with different preparations to confirm thermodynamic parameters and stoichiometry values. Binding of wild type CaM to DIII-IV in the presence of 10 mM Ca^{2+} yielded the same affinity as for 1 mM Ca^{2+}. All other ITC experiments were performed in 1 mM Ca^{2+}.

The binding isotherms were analyzed using a single site binding model using the Microcal Origin version 7.0 software package, yielding binding enthalpy (ΔH), stoichiometry (n), entropy (ΔS), and association constant (K_a). Due to the low affinity of the N-lobe interaction, very high concentrations were used (6 mM N-lobe was titrated in 600 μM DIII-IV).

Electrophysiology and Transfection—Human $Na_V1.5$ (NM_198056 (25)) and DIII-IV linker alanine mutations were generated using standard methods and were verified by DNA sequencing. The calcium phosphate method (Invitrogen) was used to transiently co-transfect tSA201 cells with channel DNA and a bicistronic vector expressing calmodulin and the CD8 marker protein to minimize the possibility that overexpression of sodium channels could exhaust the endogenous population of CaM molecules. Transfected cells were identified by binding the anti-CD8-coated beads (Invitrogen). Voltage-gated sodium currents were recorded as described previously (10). Briefly, all data were collected between 10 and 15 min after the establishment of the whole cell configuration to avoid the documented leftward shift in the steady-state inactivation gating. In this time window, no voltage-dependent drift was seen with either wild type or mutant sodium channels. Electrode resistance was in the range of 1–1.5 megaohms, and the voltage errors due to series resistance were always <3 mV after compensation. Liquid junction potentials between the bath and the pipette solution were corrected. All experiments were performed at room temperature. The patch pipette contained the following for "zero" calcium: 10 mmol/liter NaF, 100 mmol/liter CsF, 20 mmol/liter $CsCl_2$, 20 mmol/liter BAPTA, and 10 mmol/liter HEPES (pH 7.35). For 10 μM calcium, it contained the following: 10 mmol/liter NaF, 100 mmol/liter CsF, 20 mmol/liter $CsCl_2$, 1 mmol/liter BAPTA, 1 mmol/liter $CaCl_2$, 10 mmol/liter

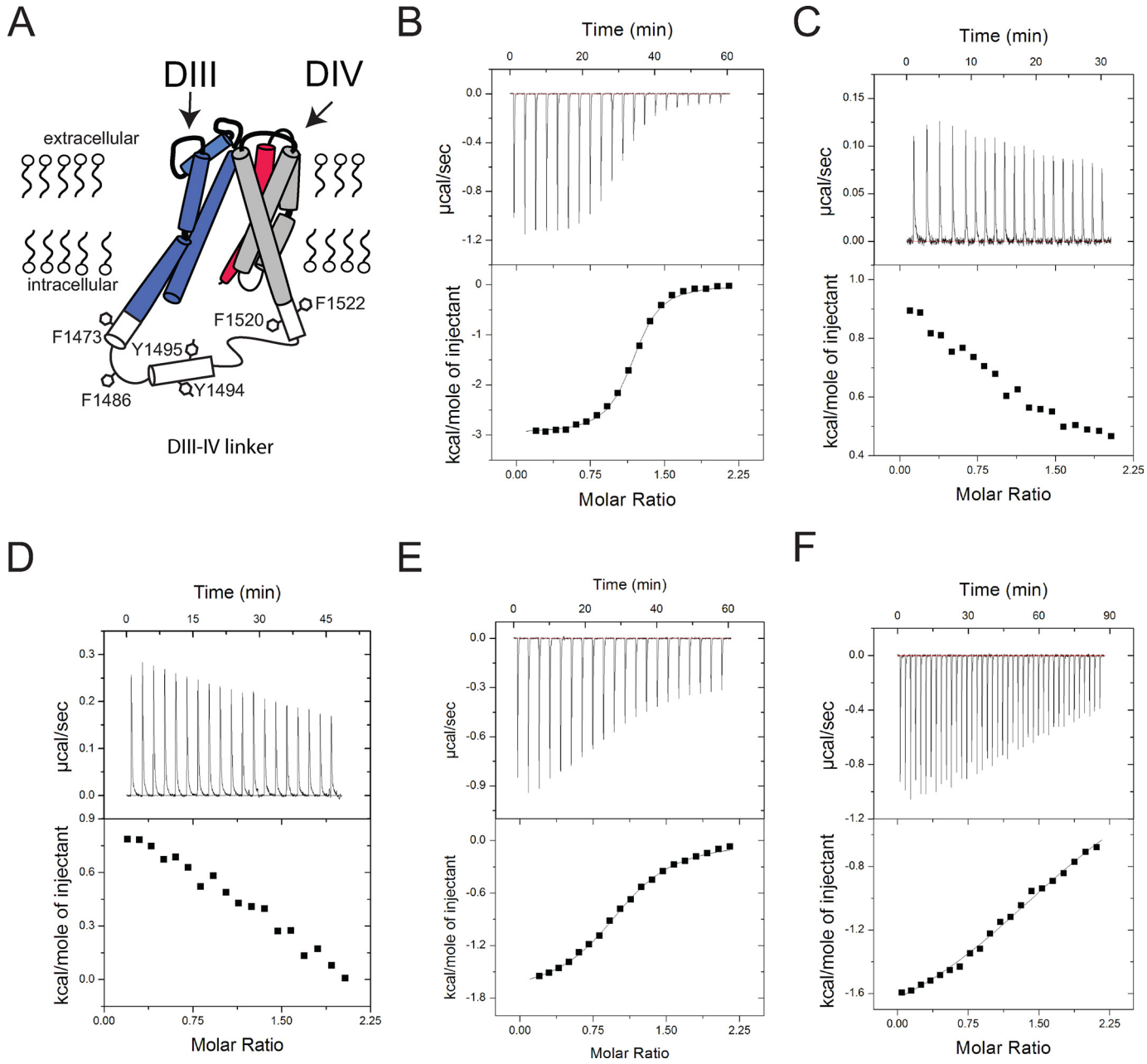

FIGURE 1. **Calmodulin binding to the sodium channel inactivation gate is calcium-dependent.** Shown is a diagram of the orientation of the DIII pore (*blue*), DIII-IV linker (*white*), and DIV voltage-sensing domain (gray (S1–S3) and *red* (S4)) with putative hydrophobic anchor points for the calmodulin interaction *highlighted*. *B–D* show ITC characterization of DIII-DIV linker interactions with calmodulin and demonstrate the calcium dependence of the interaction. *B*, 2000 μM CaM to 200 μM of linker in 10 mM $CaCl_2$. *C*, 1260 μM linker to 126 μM of CaM in 10 mM EDTA. *D*, 1170 μM CaM1234 to 117 μM of linker in 1 mM $CaCl_2$. Lobe-specific interactions with the DIII-IV linker were characterized by titration of 2000 μM C-lobe of CaM to 200 μM DIII-IV linker (*E*) and 6000 μM N-lobe of CaM to 600 μM DIII-IV linker (*F*). The results produced a binding constant of ~19 and ~595 μM for C-lobe and N-lobe, respectively.

HEPES (pH 7.35). The bath contained 150 mmol/liter NaCl, 2 mmol/liter KCl, 1.5 mmol/liter $CaCl_2$, 1 mmol/liter $MgCl_2$, and 10 mmol/liter HEPES (pH 7.4).

RESULTS

Calcium Dependence and Contribution of CaM N- and C-lobes to DIII-IV Binding—In order to better understand how intracellular calcium affects sodium channel inactivation gating, we investigated via ITC the interaction between recombinant CaM and the $Na_V1.5$ DIII-IV linker. This experimental approach is particularly advantageous because ITC provides a full cadre of thermodynamic parameters (enthalpy, entropy, ΔG, K_{app}) that contribute to the binding of two proteins. Wild type and mutant DIII-IV linker and CaM proteins were prepared as described under "Experimental Procedures" and were verified for integrity and purity by mass spectrometry before and after titrations (data not shown). Fig. 1*A* represents the transmembrane orientation and topology of the domain III pore region in *blue* (S5-S6) and the domain IV voltage sensor composed of S1–S4 in *gray* (S1–S3) and *red* (S4). The model was based on potassium channel structures and solution NMR data of the DIII-IV linker (26, 27). The DIII-IV linker aromatic

TABLE 1

Thermodynamic parameters for DIII-IV $Na_V1.5$-Ca^{2+}/CaM interactions at pH 7.4 in the presence of 1 mM $CaCl_2$

Titrations were performed with 2 μM calmodulin against 200 mM linker peptide in the cell (except for the FIF mutant, which was 133 μM). The Y1494A titration was repeated a total of three times with different preparations of protein. Errors for measurements are estimated errors based on a χ^2 minimized fit of the experimental data to a single-site binding model as implemented in Origin (see "Experimental Procedures").

	K_d	ΔH	ΔS	N value	$K_a/K_{a(\text{wild type})}$
	μM	kcal/mol	cal/mol/degree		
Wild type	3.09 ± 0.21	−2.96 ± 0.02	15.3	1.15 ± 0.01	1.00
F1473A	9.61 ± 1.58	−3.61 ± 0.11	10.9	0.87 ± 0.02	0.32
F1486A	3.57 ± 0.21	−2.92 ± 0.02	15.1	1.14 ± 0.01	0.86
Y1494A					0.00
Y1495A	8.85 ± 0.51	−1.25 ± 0.02	18.9	1.14 ± 0.01	0.35
F1520A	6.94 ± 1.00	−3.96 ± 0.08	10.3	0.94 ± 0.01	0.44
FIF → AIA	7.94 ± 1.13	−1.81 ± 0.06	17.3	0.78 ± 0.02	0.39

residues investigated in this study are *highlighted*. A representative experiment is shown in Fig. 1*B*, where CaM is titrated against the sodium channel inactivation gate composed of residues Asp^{1471}–Phe^{1522}. The data are fit with a standard binding equation yielding the thermodynamic parameters for the interaction in Table 1. In the presence of Ca^{2+}, CaM binds with a ~3 μM K_d, an interaction driven by both enthalpic and entropic contributions, confirming a previous report that CaM can bind the sodium channel DIII-IV linker with high affinity (18).

The calcium dependence of the CaM interaction with the DIII-IV linker is relevant because this characteristic would contribute to the dynamic "calcium sensing" complex that allows calcium ions to rapidly influence sodium channel inactivation gating. Alternatively, if the binding between the inactivation gate and CaM was independent of local calcium levels, such an interaction could support calcium regulation by stabilizing the channel in a conformation that is "permissive" to regulation by calcium through other channel domains. To distinguish these possibilities in terms of CaM/DIII-IV binding, the calcium dependence of the interaction was explored directly by removing calcium from the buffer used in the binding experiment. Under these conditions, we were unable to detect a significant interaction between CaM and the DIII-IV linker (Fig. 1*C*). In addition, CaM1234, a CaM mutant that cannot bind calcium in either lobes, also fails to show significant heat signals (Fig. 1*D*), showing that Ca^{2+} binding to CaM is strictly required for association with the DIII-IV linker.

Each CaM molecule contains two functional binding units in the N- and C-terminal lobes, and each is capable of interacting with target proteins. Fig. 1, *E* and *F*, shows the contribution of the isolated CaM lobes to DIII-IV linker binding. In Fig. 1*F*, 6 mM CaM N-lobe was titrated against the DIII-IV linker, and the interaction, although energetically significant, is considerably weaker ($K_d > 500$ μM) than full-length CaM (K_d ~3 μM). Conversely, the relatively robust interaction between the CaM C-lobe and the DIII-IV linker (K_d ~19 μM) is evidenced in both the quantity of released heat and the pronounced curvature of the integrated heats. The overall result demonstrates that the interaction between CaM and the sodium channel inactivation gate is strongly dependent on calcium, and this binding relies primarily on the C-lobe of CaM. The stoichiometry value for the N-lobe is close to 2, suggesting that there are two N-lobe binding sites in the DIII-IV linker. However, it is commonly observed that the N-lobe can associate with a C-lobe binding site in the absence of a C-lobe (23).

A Role for DIII-IV Aromatic Residues in Ca^{2+}/CaM Binding—Upon binding four calcium ions, CaM undergoes a conformational rearrangement that exposes hydrophobic pockets into which aromatic/hydrophobic side chains on a target protein may favorably interact. In order to determine the direct contribution of the aromatic residues shown in Fig. 1*A*, each was individually mutated to alanine, and the resulting recombinant alanine mutant DIII-IV linker peptides were assayed for their ability to bind CaM, as measured by ITC analysis. The first residue, Phe^{1473}, connects the distal pore-lining S6 segment in domain III and the amino terminus of the III-IV linker. The data in Fig. 2*A* show that the Ala mutation lowers affinity for CaM by a relatively modest ~3-fold compared with wild type. We then investigated the role of Phe^{1486}, a residue in the inactivation particle or "IFM motif" that is essential for normal inactivation gating (3). Fig. 2*B* shows that the F1486A substitution has little effect on either entropic or enthalpic contribution to CaM binding, suggesting that although this site is essential for proper inactivation gating, it does not play a direct role in CaM binding to the DIII-IV linker.

A Double Tyrosine Motif and Distal DIII-IV Linker Aromatics—A pair of aromatic residues in the cardiac sodium channel DIII-IV linker, Tyr^{1494} and Tyr^{1495}, have been implicated previously in the coupling of activation and inactivation (28) and as sites of phosphorylation by the tyrosine kinase Fyn (10). Fig. 2*C* shows that Ala replacement at these sites drastically affects the CaM/DIII-IV interaction. Due to the very low heat signals, attempts to fit the data for the Y1494A substitution were unsuccessful, showing clearly that Tyr^{1494} is involved in CaM binding. Alanine mutation at the adjacent site, Tyr^{1495}, (Fig. 2*D*) reduces the binding affinity by almost 3-fold in addition to a 2-fold loss in the ΔH of the interaction. Taken together, the data suggest that this double Tyr motif, with Tyr^{1494} in particular, contributes substantial binding energy to the interaction of the DIII-IV linker with CaM, and the energetic basis for this effect is investigated in detail below with an isolated CaM C-lobe. Recent work has suggested that the distal C terminus of the III-IV linker, in particular an "FIF" motif, is also a molecular determinant for the interaction with CaM (18). We therefore investigated the contribution of these side chains to CaM binding with a single F1520A or double F1520A/F1522A mutation. The results in Fig. 2, *E* and *F*, show that the effect on CaM binding of either the single or double mutation is surprisingly modest, suggesting that these sites play, at most, supporting roles in the interaction.

Binding of the CaM C-lobe to the DIII-IV Linker—In the presence of Ca^{2+}, CaM interacts with target proteins through the collective binding energy provided by the N- and C-terminal lobes. Although it would be mechanistically revealing to measure the contribution of each CaM lobe to DIII-IV linker binding, the data in Fig. 1*F* show that N-lobe binding is relatively weak (K_d = 595 μM), a characteristic that would preclude a complete study of alanine mutants that further lower the affinity. We therefore chose to study the interaction between an isolated C-lobe and DIII-IV linker alanine mutants, which,

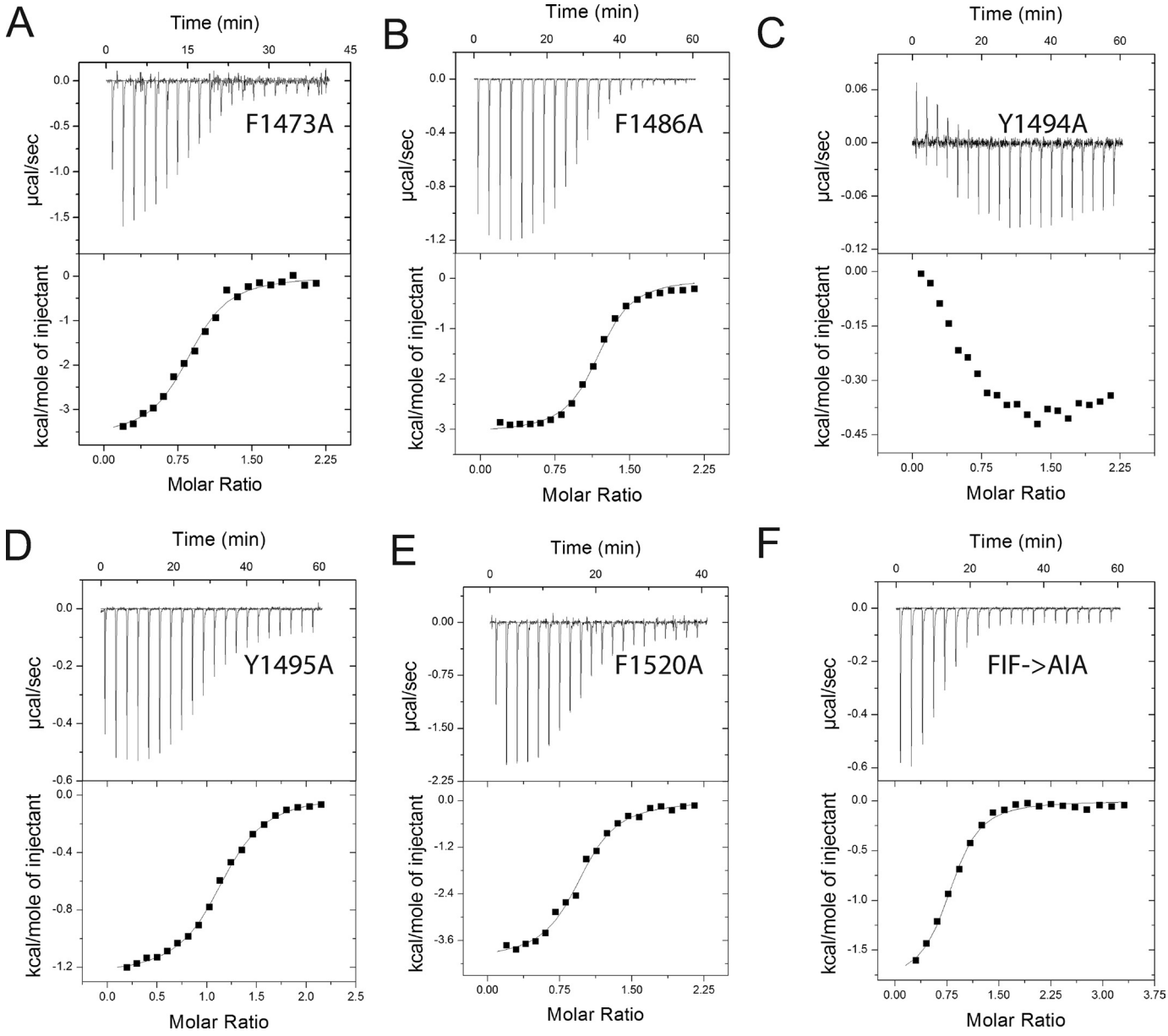

FIGURE 2. **Contributions of aromatic residues in the DIII-IV linker to CaM binding.** *A–F*, ITC traces for titration of calmodulin into the indicated wild type and mutant DIII-IV linker peptides. The thermodynamic properties of the interactions are shown in Table 1 except for Y1494A, which could not be accurately fit. Titrations with this mutant were repeated three times with different preparations of protein, and in each case the results yielded similar thermodynamic properties and binding characteristics. Mutation of the neighboring aromatic, Y1495A, produces a 3-fold loss in binding affinity and 2-fold loss in Δ*H* (Table 1) confirming a role for this site as well in CaM binding.

together with the CaM binding data, indirectly reports on the N-lobe binding. The results of the alanine scan are presented in Fig. 3, *A–F*, and show that although each mutation subtly affects the binding parameters, only the Y1494A and Y1495A substitutions have drastic effects. In both instances, the reactions become endothermic, with positive Δ*H* values of 2.74 and 1.08 kcal/mol, respectively. Surprisingly, the overall affinity is not significantly altered, thanks to a more favorable entropic contribution. This can be explained by a positive correlation, or compensation, due to a change in entropy (29). As the enthalpic contribution of the interaction becomes weaker (−1.74 kcal/mol to 2.74 kcal/mol for wild type and Y1494A, respectively), the entropy increases (15.7 cal/mol/degree to 30.8 cal/mol/degree for wild type and Y1494A, respectively) due to the relaxation of the interaction. This enthalpy/entropy compensation has also been observed for CaM C-lobe binding to a mutant of the CaV1.2 IQ domain (23). The endothermic binding now explains the low heat signals obtained for full-length CaM to the same mutants; the endothermic C-lobe binding and exothermic N-lobe binding cancel each other out. In conclusion, although both Tyr^{1494} and Tyr^{1495} form clear C-lobe anchoring sites, their individual mutations to Ala do not significantly alter the C-lobe and CaM affinities for DIII-IV, a result that would have probably been missed by traditional co-immunoprecipitation approaches.

Impact of CaM Binding to the DIII-IV Linker on Ca^{2+} Regulation of the Cardiac Sodium Channel—If the interaction between CaM and the DIII-IV linker represents a *bona fide*

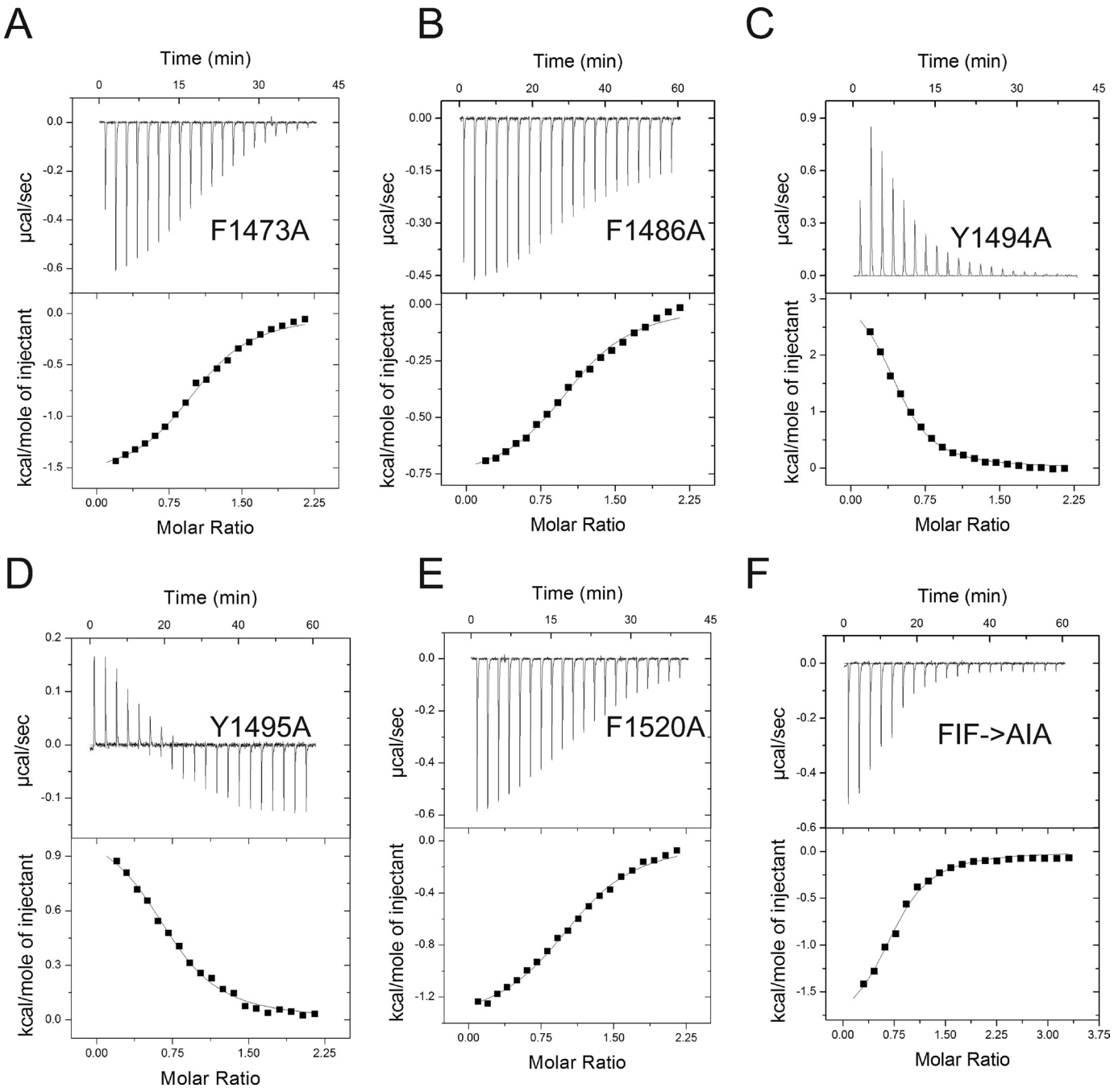

FIGURE 3. **Tyr[1494] and Tyr[1495] are CaM C-lobe binding determinants.** *A–F*, representative ITC traces for titration of C-terminal calmodulin lobe into DIII-IV linker peptides with thermodynamic properties and binding parameters shown in Table 2. The data show that the Ala substitutions are well tolerated, save Y1494A and Y1495A, which show significant endothermic binding. This endothermic binding suggests that the low heat signals obtained for full-length CaM to the same mutants, especially Y1494A, in Fig. 2 result from enthalpy/entropy compensation (see "Results" for details).

regulatory mechanism by which channel function is controlled through local calcium levels, then mutations that affect CaM binding to the DIII-IV linker should also alter the effect of calcium on channel inactivation gating. A hallmark of calcium regulation of sodium channels can be seen in the inactivation gating, where increasing cytosolic calcium causes a rightward (depolarizing) shift in the steady state availability curve (6, 11, 14, 16). The physiological consequence of this modulation is an increase in cellular excitability due to enhanced channel availability at resting membrane potentials. An example is shown in Fig. 4*A*, where sodium currents were recorded with a pipette solution containing either 10 μM free Ca^{2+} or a zero Ca^{2+} solution containing 20 mM BAPTA. A steady-state inactivation protocol was used (see *inset*), where a 200-ms prepulse from a holding potential of −140 mV to voltages from −160 to −40 mV was followed by a brief, 15-ms test pulse to −20mV to ascertain the number of channels not inactivated by the prepulse. Representative data used to generate the steady-state inactivation curves are shown as *insets* in Fig. 4, where the *arrow* indicates the test pulse measured after the −100 mV prepulse, highlighting the effect of calcium. The single Ala mutations were well tolerated and produced channels with normal gating, save the

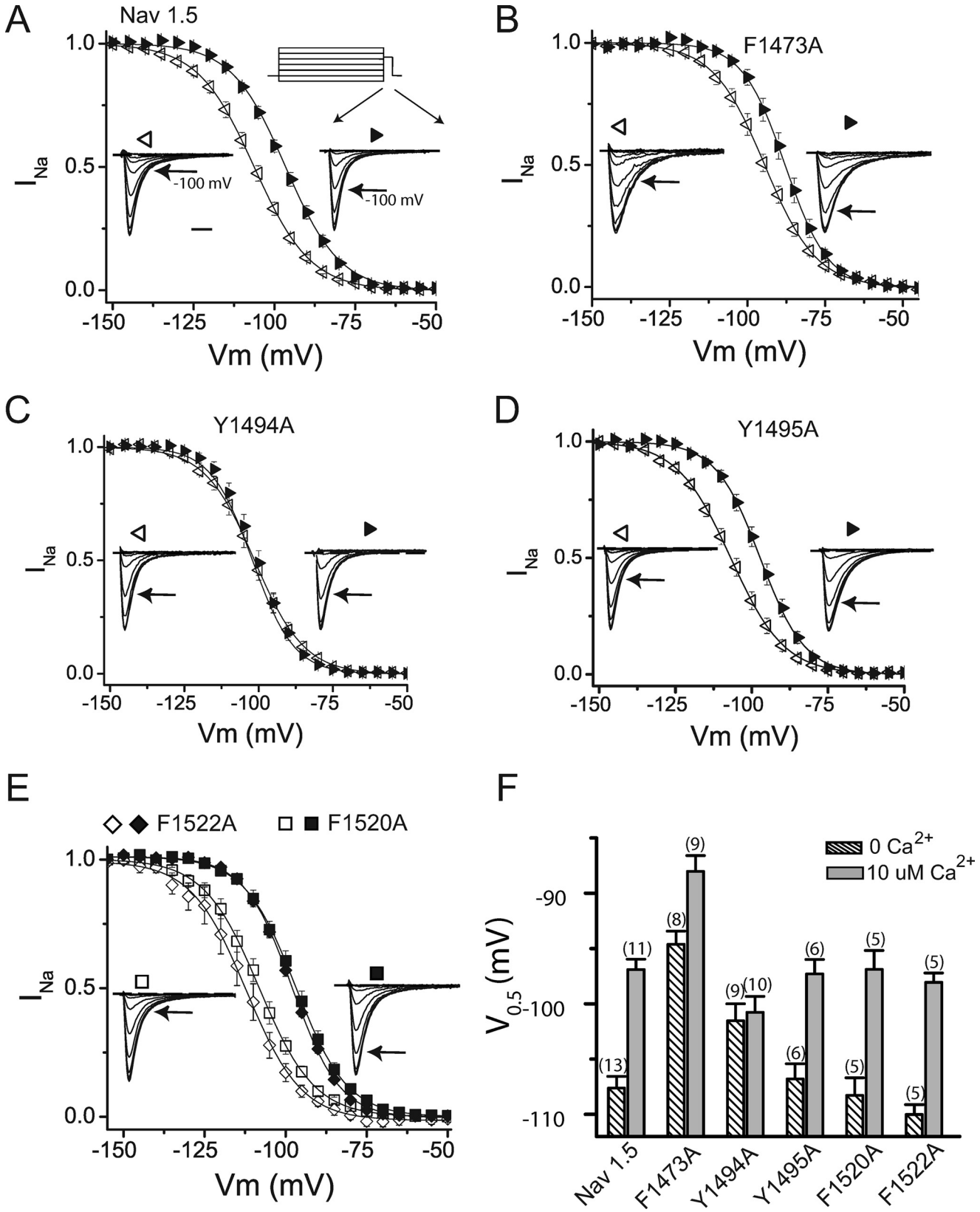

FIGURE 4. **The Y1494A mutation abolishes the calcium-dependent shift in steady-state availability of cardiac sodium channels.** *A–E* show the steady-state inactivation relationships for 0 and 10 μM Ca^{2+} in *open* and *closed symbols*, respectively. The *insets* show representative normalized sodium currents produced by the indicated channel types recorded in zero Ca^{2+}/10 μM Ca^{2+} conditions on the *left* and *right*, respectively. In all cases, the *arrow* indicates the test pulse elicited with a −100 mV prepulse. All data are shown on same time scale, with the *bar* in *A* representing 2 ms. In *E*, only data from F1520A-expressing cells are presented for clarity. *Inset*, data were attained using the protocol described for Fig. 4*A*, where cells were held at −140 mV, depolarized to a variable prepulse for 200 ms before a 15-ms test pulse to −20 mV. The data are summarized in *F*, where the $V_{0.5}$ of each channel type is plotted for 0 and 10 μM Ca^{2+}. All channel types except Y1494A showed a significant shift in inactivation gating ($p < 0.005$; see Table 3).

TABLE 2

Thermodynamic parameters for DIII-IV $Na_V1.5$-CaM C-lobe interactions at pH 7.4 in the presence of 1 mM $CaCl_2$

Titrations were performed with 2 mM calmodulin in the syringe and 200 μM linker peptide in the cell (except for the FIF mutant, which was 133 μM). Errors for measurements are estimated errors based on a χ^2 minimized fit of the experimental data to a single-site binding model as implemented in Origin (see "Experimental Procedures").

	K_d	ΔH	ΔS	N value	$K_d/K_{d(\text{wild type})}$
	μM	kcal/mol	cal/mol/degree		
Wild type	19.27 ± 0.94	−1.74 ± 0.02	15.7	1.04 ± 0.01	1.00
F1473A	19.88 ± 1.95	−1.60 ± 0.03	16.2	1.05 ± 0.02	0.97
F1486A	16.76 ± 1.45	−1.68 ± 0.04	16.2	0.80 ± 0.02	1.15
Y1494A	19.08 ± 1.43	2.74 ± 0.06	30.8	0.73 ± 0.01	1.01
Y1495A	24.88 ± 2.82	1.08 ± 0.04	24.7	0.73 ± 0.02	0.77
F1520A	25.44 ± 2.21	−1.39 ± 0.03	16.3	1.11 ± 0.02	0.76
FIF → AIA	18.21 ± 2.62	−1.93 ± 0.11	15.2	0.74 ± 0.03	1.06

TABLE 3

Parameters from Boltzmann fits of steady-state inactivation gating for wild-type $Na_V1.5$ and DIII-IV linker alanine mutants

The number of cells is shown in parentheses. All channel types except for Y1494A show a calcium-dependent shift in the voltage dependence of inactivation gating. The impact of calcium on the slope factor, k, was more modest and was significant for only F1473A, Y1494A, and Y1495A.

	0 μM Ca^{2+}		10 μM Ca^{2+}	
	$V_{0.5}$	k	$V_{0.5}$	k
	mV		mV	
Wild type $Na_V1.5$	−109.4 ± 0.7 (7)	8.8 ± 0.2	−97.1 ± 1.0 (9)[a]	8.1 ± 0.3
F1473A	−94.6 ± 1.2 (8)	8.1 ± 0.3	−88.0 ± 1.4 (9)[a]	6.3 ± 0.1[a]
Y1494A	−101.5 ± 1.5 (9)	7.6 ± 0.3	−100.7 ± 1.4 (10)	6.3 ± 0.1[a]
Y1495A	−106.8 ± 1.4 (6)	8.6 ± 0.1	−97.3 ± 0.96 (6)[a]	7.0 ± 0.2[a]
F1520A	−108.3 ± 0.2 (5)	8.3 ± 0.2	−96.9 ± 1.1 (5)[a]	8.3 ± 0.2
F1522A	−110.0 ± 0.6 (5)	8.0 ± 0.4	−98.1 ± 0.6 (5)[a]	7.3 ± 0.06

[a] Student's t test $p < 0.005$ versus 0 μM Ca^{2+}.

F1473A mutation, which displayed a small "residual" sodium current consistent with previous mutagenesis (30) and decreased current expression (data not shown). Fig. 4*B* shows that this gating alteration aside, this mutant was still significantly modulated by calcium ($p > 0.005$; see Table 2), but the effect was reduced in comparison with wild type channels. This is consistent with the slightly altered affinity (~3-fold less) of CaM for this mutant. Contrary to the modest effect of this mutation, Fig. 4*C* shows that Ala replacement at the Tyr^{1494} site abolished the calcium sensitivity of sodium channel inactivation gating. Although the Tyr^{1494} mutation is clearly involved in CaM binding, the result is unexpected because it does not affect the overall affinity of CaM or C-lobe binding. This suggests that generic CaM binding to the DIII-IV linker region is not enough on its own to impact channel inactivation and that specific interaction with Tyr^{1494} is required. In contrast, the site one amino acid downstream, Y1495A, showed a robust calcium response that was completely normal in magnitude and direction compared with wild type, despite the fact that the effect on CaM and C-lobe binding is similar to the Y1494A mutation. One way to reconcile these results is to conclude that Tyr^{1494} is directly involved in both the inactivation mechanism *and* CaM binding, whereas Tyr^{1495} only contributes to the latter. This possibility is supported by the destabilization of inactivation that is seen with either CaM binding to or mutation of Tyr^{1494} to alanine, two manipulations that similarly cause a rightward shift in steady-state inactivation (see "Discussion"). Last, the F1520A and F1522A mutations produce channels that are fully sensitive to free calcium (Fig. 4*E*), further moving focus from them as either a molecular determinant of CaM binding or of calcium modulation. The results of the effects on inactivation gating are summarized in Fig. 4*F*, where the $V_{0.5}$ for the steady-state inactivation is plotted for each channel type in 0 or 10 μM free calcium. All of the constructs tested, save Y1494A, showed a significant shift in the $V_{0.5}$ between the two calcium conditions ($p < 0.005$; see Table 3). Last, the effect of calcium on the decay kinetics for these sodium channels is shown in supplemental Fig. S2. Here, calcium generally had a small but statistically insignificant ($p > 0.005$) impact on decay kinetics except for Y1494A, where a pronounced slowing of inactivation in zero calcium recording solution was seen at depolarized potentials. We hypothesize that this effect is caused by the altered CaM binding to the DIII-IV linker predicted by our ITC analysis of this mutant.

DISCUSSION

Intracellular calcium is a potent regulator of cardiac sodium channel inactivation gating. Calmodulin has been shown previously to bind to the sodium channel DIII-IV linker, and the interaction could be supported, at least partially, by the contribution of the three hydrophobic residues Phe^{1520}–Phe^{1522} (18). However, the construct used to identify these residues contained only the distal C-terminal residues of the DIII-IV linker, lacking the double Tyr motif we identify here and notably including residues that make up the putative D4S1 transmembrane segment region. Although CaM binding to a transmembrane segment presents interesting mechanistic possibilities, it must also be considered that the proposed CaM binding sites may be unavailable in the context of a full-length channel. Further, the previously reported binding may be due, in part, to spurious interactions between hydrophobic pockets on CaM and hydrophobic residues that are only available *in vitro*. To avoid such complicating factors, here we decided to look at binding of CaM to a DIII-IV linker construct that does not include any putative transmembrane regions. With this approach, we have made three novel observations toward the molecular understanding of the effect of Ca^{2+} on sodium channel gating. First, we show that calcium must be present and in complex with CaM prior to binding the sodium channel inactivation gate. This suggests that CaM and the DIII-IV linker comprise a dynamic calcium sensor that, including the carboxyl terminus of the channel, form a complex that is ideally placed to modulate cardiac sodium channel gating on a beat-by-beat basis. Second, a double tyrosine motif at Tyr^{1494}/Tyr^{1495} in the DIII-IV linker forms an anchor for CaM binding by stabilizing the interaction with the CaM C-lobe. These residues lie well outside of the predicted CaM binding site composed of the distal DIII-IV linker "FIF" residues and the putative DIV segment 1 transmembrane segment suggested by the Calmodulin Target Database (18, 31). The results, therefore, demonstrate that the sodium channel inactivation gate is an atypical CaM binding sequence. Last, the combined ITC and electrophysiological data suggest that "generic" CaM binding to the DIII-IV linker alone cannot facilitate calcium-dependent modulation of inactivation gating. We base this conclusion on the experimental observation that the Y1494A mutation alters the binding dynamics with CaM but does not abolish the interaction altogether and produces a channel incapable of calcium modula-

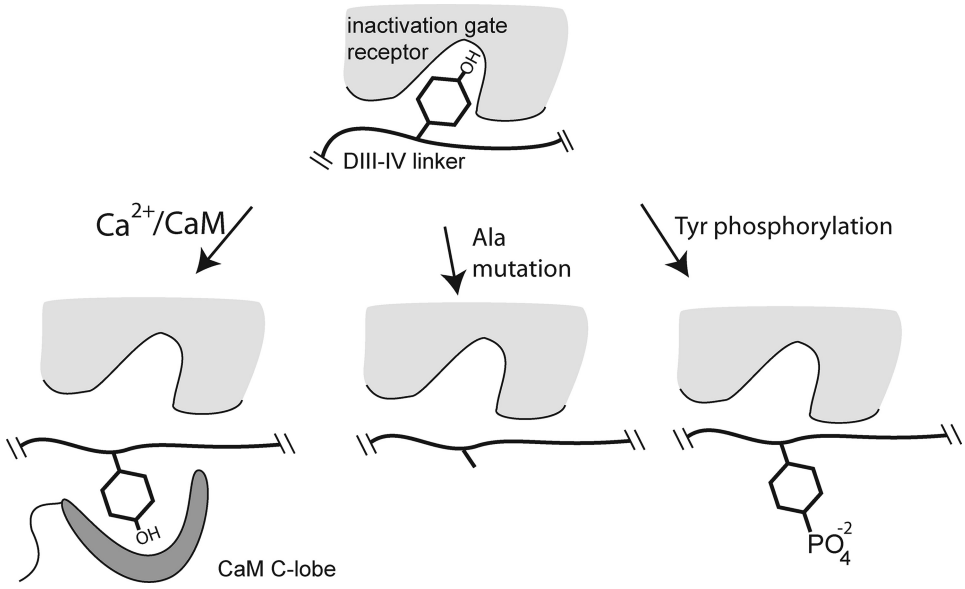

FIGURE 5. **Working model for the role of Tyr^{1494} in Ca^{2+}/CaM regulation, inactivation, and tyrosine phosphorylation.** We propose that Tyr^{1494} assists in stabilizing the inactivated state of the channel by interacting with residues that make up the inactivation gate receptor. The data suggest that the three manipulations shown here destabilize the inactivated state by interfering with the ability of Tyr^{1494} to bind to the inactivation gate receptor either through antagonism by Ca^{2+}/CaM, outright removal of the side chain, or in the case of Tyr^{1495}, disruption of receptor binding by phosphorylation. It is assumed that phosphorylation of Tyr^{1495} would negatively impact CaM binding. The *middle panel* summarizes the only effects of the Y1494A mutation on inactivation in the absence of a bound CaM molecule.

tion. Further, our results suggest that Tyr^{1494} is a residue directly involved in inactivation; substitution by Ala shifts the inactivation curve to the right in the absence of Ca^{2+}, whereas the addition of further Ca^{2+} does not produce any extra shift.

The combined results of the ITC and electrophysiology data therefore suggest the following model (Fig. 5). Tyr^{1494}, in addition to other DIII-IV linker residues, promotes inactivation through binding residues in or near the transmembrane region, which may be composed of the short cytosolic S4-S5 linkers connecting the voltage sensors and gates in domains III and IV (4, 5). Elevation of cytoplasmic Ca^{2+} levels leads to binding of Ca^{2+}/CaM, resulting in shielding of Tyr^{1494} (and Tyr^{1495}) by the CaM C-lobe, which is therefore unable to promote inactivation. The same effect can be obtained by simple substitution of Tyr^{1494} to alanine, shown in the *middle panel*. This model also explains previous results showing that the cardiac sodium channel inactivation gating is modulated by the tyrosine kinase Fyn, where both Tyr^{1494} and Tyr^{1495} can be phosphorylated *in vitro* and the effect of phosphorylation was a depolarizing shift in the steady-state inactivation, the same as increased intracellular calcium. It would be expected that phosphorylation of the two Tyr residues would serve to diminish or inhibit CaM binding, in addition to altering the interaction of the side chain with the inactivation gate receptor. It is therefore noteworthy that Ca^{2+}/CaM and CaMKII have been implicated in the appearance of a late sodium current in failing myocardium (22), and such conditions can include a rise in tyrosine phosphorylation activity (32). However, it should be noted that neither we nor others (14, 16) observe a late sodium current in either zero calcium or low calcium recording solutions (supplemental Fig. S1), ruling out a direct role for the calcium-dependent CaM binding that we describe here to the DIII-IV linker in its generation.

SomeparallelsexistbetweenCa^{2+}-dependent regulation of voltage-gated sodium and calcium channels (Ca_V). Ca_V channels of the Ca_V1 and Ca_V2 families can undergo two types of Ca^{2+}-dependent feedback mechanisms, calcium-dependent inactivation and calcium-dependent facilitation, mediated through CaM binding at various sites in the channel (33). These include a pre-IQ and IQ domain in the proximal C-terminal tail (23, 34–36) and a site at the N terminus of some channel types (37). However, the Ca_V III-IV loop has thus far not been described as a CaM-interacting region. A recent crystal structure, including the $Ca_V1.2$ pre-IQ and IQ region in complex with CaM as a domain-swapped dimer shows that two CaM molecules can bind the channel simultaneously (36). Because both the IQ domain and DIII-IV linker of $Na_V1.5$ can bind CaM, it will be interesting to see whether either single or multiple CaMs are involved in $Na_V1.5$ modulation.

Many residues in the sodium channel inactivation gate, including the double tyrosine CaM binding motif described here, are conserved between the nine known sodium channel voltage-gated isoforms. Therefore, the mechanism of Ca^{2+}/CaM binding to the double Tyr motif described here is probably utilized not only by the cardiac isoform but also by sodium channel isoforms expressed in the central and peripheral nervous systems.

Acknowledgment—We thank Ana Niciforovic for expert technical assistance.

REFERENCES

1. Horn, R., Patlak, J., and Stevens, C. F. (1981) *Nature* **291,** 426–427
2. Joseph, D., Petsko, G. A., and Karplus, M. (1990) *Science* **249,** 1425–1428
3. West, J. W., Patton, D. E., Scheuer, T., Wang, Y., Goldin, A. L., and Catterall, W. A. (1992) *Proc. Natl. Acad. Sci. U.S.A.* **89,** 10910–10914
4. Smith, M. R., and Goldin, A. L. (1997) *Biophys. J.* **73,** 1885–1895
5. McPhee, J. C., Ragsdale, D. S., Scheuer, T., and Catterall, W. A. (1998) *J. Biol. Chem.* **273,** 1121–1129
6. Tan, H. L., Kupershmidt, S., Zhang, R., Stepanovic, S., Roden, D. M., Wilde, A. A., Anderson, M. E., and Balser, J. R. (2002) *Nature* **415,** 442–447
7. Kass, R. S. (2006) *J. Cardiovasc. Electrophysiol.* **17,** Suppl. 1, S21–S25
8. Grieco, T. M., Malhotra, J. D., Chen, C., Isom, L. L., and Raman, I. M. (2005) *Neuron* **45,** 233–244
9. West, J. W., Numann, R., Murphy, B. J., Scheuer, T., and Catterall, W. A. (1991) *Science* **254,** 866–868
10. Ahern, C. A., Zhang, J. F., Wookalis, M. J., and Horn, R. (2005) *Circ. Res.* **96,** 991–998
11. Young, K. A., and Caldwell, J. H. (2005) *J. Physiol.* **565,** 349–370

12. Deschênes, I., Neyroud, N., DiSilvestre, D., Marbán, E., Yue, D. T., and Tomaselli, G. F. (2002) *Circ. Res.* **90,** E49–E57
13. Wingo, T. L., Shah, V. N., Anderson, M. E., Lybrand, T. P., Chazin, W. J., and Balser, J. R. (2004) *Nat. Struct. Mol. Biol.* **11,** 219–225
14. Kim, J., Ghosh, S., Liu, H., Tateyama, M., Kass, R. S., and Pitt, G. S. (2004) *J. Biol. Chem.* **279,** 45004–45012
15. Mori, M., Konno, T., Ozawa, T., Murata, M., Imoto, K., and Nagayama, K. (2000) *Biochemistry* **39,** 1316–1323
16. Biswas, S., DiSilvestre, D., Tian, Y., Halperin, V. L., and Tomaselli, G. F. (2009) *Circ. Res.* **104,** 870–878
17. Motoike, H. K., Liu, H., Glaaser, I. W., Yang, A. S., Tateyama, M., and Kass, R. S. (2004) *J. Gen. Physiol.* **123,** 155–165
18. Potet, F., Chagot, B., Anghelescu, M., Viswanathan, P. C., Stepanovic, S. Z., Kupershmidt, S., Chazin, W. J., and Balser, J. R. (2009) *J. Biol. Chem.* **284,** 8846–8854
19. George, A. L., Jr. (2005) *J. Clin. Invest.* **115,** 1990–1999
20. Viswanathan, P. C., and Balser, J. R. (2004) *Trends Cardiovasc. Med.* **14,** 28–35
21. Wagner, S., Dybkova, N., Rasenack, E. C., Jacobshagen, C., Fabritz, L., Kirchhof, P., Maier, S. K., Zhang, T., Hasenfuss, G., Brown, J. H., Bers, D. M., and Maier, L. S. (2006) *J. Clin. Invest.* **116,** 3127–3138
22. Maltsev, V. A., Reznikov, V., Undrovinas, N. A., Sabbah, H. N., and Undrovinas, A. (2008) *Am. J. Physiol. Heart Circ. Physiol.* **294,** H1597–H1608
23. Van Petegem, F., Chatelain, F. C., and Minor, D. L., Jr. (2005) *Nat. Struct. Mol. Biol.* **12,** 1108–1115
24. Edelhoch, H. (1967) *Biochemistry* **6,** 1948–1954
25. Gellens, M. E., George, A. L., Jr., Chen, L. Q., Chahine, M., Horn, R., Barchi, R. L., and Kallen, R. G. (1992) *Proc. Natl. Acad. Sci. U.S.A.* **89,** 554–558
26. Long, S. B., Campbell, E. B., and Mackinnon, R. (2005) *Science* **309,** 897–903
27. Rohl, C. A., Boeckman, F. A., Baker, C., Scheuer, T., Catterall, W. A., and Klevit, R. E. (1999) *Biochemistry* **38,** 855–861
28. O'Leary, M. E., Chen, L. Q., Kallen, R. G., and Horn, R. (1995) *J. Gen. Physiol.* **106,** 641–658
29. Dunitz, J. D. (1995) *Chem. Biol.* **2,** 709–712
30. Bankston, J. R., Yue, M., Chung, W., Spyres, M., Pass, R. H., Silver, E., Sampson, K. J., and Kass, R. S. (2007) *PLoS One* **2,** e1258
31. Yap, K. L., Kim, J., Truong, K., Sherman, M., Yuan, T., and Ikura, M. (2000) *J. Struct. Funct. Genomics* **1,** 8–14
32. Melillo, G., Lima, J. A., Judd, R. M., Goldschmidt-Clermont, P. J., and Silverman, H. S. (1996) *Circulation* **93,** 1447–1458
33. Chaudhuri, D., Issa, J. B., and Yue, D. T. (2007) *J. Gen. Physiol.* **129,** 385–401
34. Fallon, J. L., Halling, D. B., Hamilton, S. L., and Quiocho, F. A. (2005) *Structure* **13,** 1881–1886
35. Kim, E. Y., Rumpf, C. H., Fujiwara, Y., Cooley, E. S., Van Petegem, F., and Minor, D. L., Jr. (2008) *Structure* **16,** 1455–1467
36. Fallon, J. L., Baker, M. R., Xiong, L., Loy, R. E., Yang, G., Dirksen, R. T., Hamilton, S. L., and Quiocho, F. A. (2009) *Proc. Natl. Acad. Sci. U.S.A.* **106,** 5135–5140
37. Dick, I. E., Tadross, M. R., Liang, H., Tay, L. H., Yang, W., and Yue, D. T. (2008) *Nature* **451,** 830–834